nature portfolio

Peer Review File

High-performance Microelectronic-integratable Molecular Transistor

Corresponding Author: Professor Yuan Li

This file contains all reviewer reports in order by version, followed by all author rebuttals in order by version.

Version 0:

Reviewer comments:

Reviewer #3

(Remarks to the Author)
This manuscript, entitled “High-Performance Microelectronic-Integratable Molecular Transistors,” reports molecular transistors based on Au–SAM//single-layer graphene (SLG) vertical heterostructures gated by ionic liquids, achieving ON/OFF ratios exceeding 104 at temperatures up to 350 K. The authors further demonstrate the implementation of logic gates and wafer-scale (~2 inch) device integration. The overall concept is clearly articulated, and the reported device performance represents a significant advancement compared to previously reported molecular transistors. The emphasis on microelectronic compatibility is particularly appealing and aligns well with the scope and readership of Nature Communications. However, several major scientific aspects require further clarification and more in-depth discussion before the manuscript can be considered for acceptance. These points are outlined below:

Major revision:
1. The authors attribute the device switching to ionic-liquid-gated electric-field penetration through SLG, enabling modulation of molecular frontier orbitals. The initial HOMO/LUMO alignment relative to the SLG Fermi level (~±0.2–0.4 eV) is used as the key justification. However, the observed gate modulation may alternatively arise from:
Graphene carrier-density tuning or Gate-induced modification of SLG–molecule contact barriers. Please add control experiments using Ionic-liquid-gated SLG without SAM, or thinner conventional dielectrics, these would help isolate the molecular contribution.
2. The electrical performance of the reported devices relies critically on the structural integrity, coverage, and ordering of the self-assembled monolayer (SAM) confined inside the micropores. However, the current manuscript provides very limited direct evidence for the quality of the molecular junction. The vertical gap thickness is inferred primarily from a single high-resolution TEM image showing an apparent ~1.5 nm separation, which may also contain contributions from residual oxide, contamination, or voids, and therefore cannot unambiguously confirm the presence of a well-formed, densely packed SAM. Please provide additional and more direct characterization of the SAM, such as X-ray photoelectron spectroscopy, ellipsometry, infrared reflection–absorption spectroscopy (IRRAS), or contact angle measurements, to verify thiol anchoring, molecular coverage, and monolayer thickness.
3. Furthermore, statistical information on the micropore geometry (diameter, depth, and residual dielectric thickness), obtained from cross-sectional SEM, AFM, or multiple TEM images, is necessary to establish the uniformity of the vertical junctions and to rationalize device-to-device current variations.
4. Additionally, since multiple molecular species (exTTF, C60, Fc, and PDI derivatives) are employed, a comparative discussion of their respective SAM quality and packing behavior would significantly strengthen the structural interpretation of the electrical results.
5. The manuscript claims wafer-scale integration of approximately 8000 molecular transistors on a 2-inch wafer with an impressive reported yield of 94.8%; however, the definition of “yield” adopted here is overly permissive and does not adequately reflect true functional performance. At present, devices are classified as “working” primarily based on the observation of nonlinear I–V characteristics, which essentially confirms that the junctions are not electrically shorted but does not guarantee transistor-like switching behavior. A more rigorous distinction should be made between physical electrical yield (non-shorted junctions) and functional transistor yield defined by a minimum ON/OFF ratio, subthreshold slope, or transconductance.
6. In addition, the statistical analysis presented in Fig. 5e is internally inconsistent, where the reported average value of log (ON/OFF) and its standard deviation appear numerically implausible and require careful re-evaluation and clarification. The current statistics also seem to be obtained from a limited subset of devices on a single wafer. To support the strong claims of

wafer-scale manufacturability, the authors should present spatially resolved ON/OFF maps across the entire wafer and, ideally, include wafer-to-wafer reproducibility over multiple fabrication runs. Without such rigorous statistical treatment, the claims of high-yield, large-scale integration remain insufficiently substantiated.

Minor revision:
1. Several minor issues regarding presentation, notation, and clarity should also be addressed to improve the overall readability and accuracy of the manuscript. For example, there are evident inconsistencies in figure numbering and cross-referencing, particularly in the wafer-scale integration section where the figure labeled as “Figure 4” should correspond to “Figure 5,” and multiple internal references appear inconsistent.

Reviewer #4

(Remarks to the Author)
This manuscript reports high-performance vertical SAM-based molecular transistors using an ionic-liquid electrochemical gate. The authors show that drain-current modulation is governed by molecular-orbital/graphene-Fermi-level alignment, enabling a clear classification of HOMO- and LUMO-type molecular transistors with an intuitive p/n-type analogy. Moreover, the work demonstrates ON/OFF ratios >10^4 at and above room temperature, >100,000-cycle stability, and >90% fabrication yield, together with dense arrays on a 2-inch wafer and functional logic-gate demonstrations. Overall, the technological achievements presented here are impressive. I recommend minor revision before acceptance of Nature Communications, while some concerns regarding the theoretical interpretation of the transport mechanism and the rigorousness of the integration demonstration have been addressed.
1. The theoretical modeling appears to predict an opposite trend compared to the experimental data, which raises concerns regarding the validity of the proposed transport mechanism. Specifically, the calculated transmission spectra and current-voltage curves (Fig.2c-2d) suggest that the Au-S-exTTF//SLG junction should exhibit higher conductivity than Au-S-C60//SLG system. However, the experimental results demonstrate significantly higher current densities for the C60-based junctions. This qualitative discrepancy suggests that the theoretical model (likely based on a single-molecule junction approximation) may not be representative of the actual experimental setup. Could this mismatch be attributed to intermolecular interactions that are absent in the single-molecule calculation? The authors should provide a detailed discussion or additional calculations to reconcile this contradiction.
2. Another concern is, according to the calculated transmission spectrum for the Au-S-exTTF//SLG junction, the transport characteristics are expected to exhibit a V-shaped (ambipolar) evolution or a non-monotonic trend as the gate voltage shifts the Fermi level across the transmission features.
3. The demonstration of wafer-scale integration (Fig. 5) is arguably the most significant breakthrough of this work. However, in Figure 4, the illustration and optical images of the HOMO- and LUMO-type transistors used to create the NOT gate appear to stem from separate regions or discrete devices that were potentially wired together externally, rather than being integrated side-by-side in a compact circuit layout. To prove the robustness of their fabrication process and the feasibility of true integration, the authors should demonstrate the logic gates (e.g., the NOT gate) directly within the wafer-scale array shown in Fig. 5. Demonstrating adjacent, lithographically defined p-type and n-type devices functioning as a logic unit on the same wafer coordinates would significantly strengthen the claim of large-scale integration.
4. The authors evaluate the charge transport mechanism (via temperature-dependent measurements) for exTTF-SH junctions at a fixed bias of Vds = +0.5 V. However, I note that Figures 4a-b do not appear to present the data at this specific voltage range, creating a disconnect between the device characterization and the mechanism analysis. Since the Au-S-exTTF//SLG junction is structurally and electronically asymmetric, it is scientifically unsound to assume that the transport mechanism at derived at Vds = 0.5V applies to the negative bias regime in Fig.4a-b.

Reviewer #5

(Remarks to the Author)

This works is a nice effort towards the implementation of robust molecular transistors. The work encompasses the most important aspects enabling molecular transistors applications such as stability and scalability, which are today limiting their real world applications. The transistor operation relies on the well-known principle allowing switching molecular transport regime between off-resonant tunnelling and 1-level hopping via a redox functional group engineered into the active molecular backbone. The engineering approach to stabilise the active molecular layer into a micrometre size pore feature using a single-layer graphene top contact is clever and brings advantages towards the scalability of the process and integration in current microfab methods. All in all, I feel this will be a nice contribution to the field with wide impact on the microelectronics community.

Prior to publication of the work, I do have a few queries and clarifications for the authors I am listing below:

- I find the concept of SAM ill-defined here. There is no way molecular structures like the ones used in this work will form a nice compact monolayer as it seems to be suggested in different passages of the manuscript. The HRTEM images showing a small gap are no proof of the structural integrity of the molecular layer, which will surely bear plenty of defects, vacancies, etc. To be fair, I think a small paragraph stating how this can affect device operation and/or they can be overcome thanks to the device structure needs to be incorporated.

- Fig. 1e oversimplifies the electronic structure of the graphene layer. As part of the device manufacturing, the graphene is layer seems to be etched into some sort of nanoribbons which surely will increase the existing electronic gap of graphene.

This would affect the observed transistor operation and should be incorporated as part of the discussion of results.

- The exponential portion of the intended Arrhenius plot in S14b needs explanation.
- The asymmetry of the IVs in Fig. 2a is hard to see considering the dispersion. This questions its role in the observed transistor effect. Is the asymmetry stronger at higher voltage biases? How is this poor asymmetry translated to the strong ON-OFF transistor behaviour?

- A more detailed explanation on how the gate voltage is applied via the IL medium is needed. Is there an external reference electrode immersed in the IL drop? This is not clear from the device schemes.

- Transistor curves in Figs. 3a and c show a general lift as the gate voltage increases. While this is clear of the ON state which is based on a hopping mechanism, the increasing “leakage” current observed in the tunnelling-based OFF state is not so obvious. Explain please.

- The poor ON-OFF behaviour recorded for the C8 control is not so obvious to me as in Fig. S20 a significant ON-OFF ratio is recorded. This clashes with the idea of a molecular component providing essentially electron tunnelling through out all voltage window. Please explain.

- While the conducted study here points to an all-electric operation principle for the molecular transistor, given the structural complexity of the molecular layers, likely defective, charging effects induced by the voltage gate could possibly lead to structural changes in the layer due to electrostatic effects which would point to structurally-induced gating effects in the transistor operation. The above discussion MUST be part of the conclusions.

Version 2:

Reviewer comments:

Reviewer #3

(Remarks to the Author)
This revised manuscript “High-performance Microelectronic-integratable Molecular Transistors” by Y. Xie, et.al, reports ionic-liquid-gated molecular transistors based on Au–SAM/single-layer graphene (SLG) vertical heterostructures, demonstrating high ON/OFF ratios (>10^4), stable operation at and above room temperature, and wafer-scale device integration. The authors further implement logic gate functionality, highlighting the potential of this system for bridging molecular electronics with microelectronic compatible device platforms. The concerns raised by the reviewers are well addressed in the revised version.

While the manuscript is already of high quality and close to publication standard, a minor refinement in the presentation could further enhance its clarity and rigor. In particular, even though the expanded control experiments strongly support the interpretation that the gate modulation is dominated by molecular orbital alignment, the current evidence is better described as being consistent with this mechanism rather than strictly excluding all alternative contributions. A slight moderation of the language (for example, replacing “rule out” in line 184 with “consistent with” or “suggest”) and a brief acknowledgment of possible secondary contributions from graphene-related effects would significantly improve the balance and precision of the discussion.

I therefore recommend acceptance after addressing these above-mentioned minor concerns.

Reviewer #4

(Remarks to the Author)
The authors have carefully addressed all the concerns raised in the previous review round.I have no further questions or comments.In my opinion, the manuscript is now suitable for publication in its present form, and I recommend acceptance.

Reviewer #5

(Remarks to the Author)
I have read the responses given to my queries and to those from other reviewers , and I am happy with the answers provided and the modifications introduced in the manuscript accordingly, which have now significantly improved the clarity of many technical aspects related to the work. Thanks

Response to Reviewer Comments

Reviewer #3 (Remarks to the Author):

This manuscript, entitled "High-Performance Microelectronic-Integratable Molecular Transistors," reports molecular transistors based on Au–SAM//single-layer graphene (SLG) vertical heterostructures gated by ionic liquids, achieving ON/OFF ratios exceeding 104 at temperatures up to 350 K. The authors further demonstrate the implementation of logic gates and wafer-scale (~2 inch) device integration. The overall concept is clearly articulated, and the reported device performance represents a significant advancement compared to previously reported molecular transistors. The emphasis on microelectronic compatibility is particularly appealing and aligns well with the scope and readership of Nature Communications. However, several major scientific aspects require further clarification and more in-depth discussion before the manuscript can be considered for acceptance. These points are outlined below:

Response: We are pleased that the referee found the concept clearly articulated and we appreciate that the referee acknowledges the significant advance in device performance beyond current molecular transistors and the essential microelectronic compatibility of our demonstrated nanoscale semiconductor device. We are grateful for the recommendation to consider for publication following revision based on the reviewer's expert comments.

Major revision:

1. The authors attribute the device switching to ionic-liquid-gated electric-field penetration through SLG, enabling modulation of molecular frontier orbitals. The initial HOMO/LUMO alignment relative to the SLG Fermi level (~±0.2–0.4 eV) is used as the key justification. However, the observed gate modulation may alternatively arise from:

Graphene carrier-density tuning or Gate-induced modification of SLG–molecule contact barriers.

Please add control experiments using Ionic-liquid-gated SLG without SAM, or thinner conventional dielectrics, these would help isolate the molecular contribution.

Response: We thank the referee for this insightful comment. We used two sets of control experiments to isolate the molecular contribution: (a) an unfunctionalized SAM with just

alkanethiol (the HOMO and LUMO level are far away from the SLG Fermi level, >2 eV away), so a different molecule albeit of similar length to exTTF-SH and C_{60}-SH, and (b) the Au//SLG junction without SAMs as the referee suggested.

a) In **Section S4.1 Two-terminal molecular junctions** of **Supplementary Information**, we compared the electrical behavior of Au-S-exTTF//SLG and Au-S-C_{60}//SLG junctions with that of control Au-S-C_{18}//SLG. The exTTF-SH and C_{60}-SH molecular junctions exhibited functional, asymmetric current characteristics under positive and negative bias (**Fig. S13**), while junctions based on C_{18}-SH exhibit current characteristics independent of bias polarity (**Fig. S16a**). Furthermore, the current of Au-S-exTTF decreases with decreasing temperature, indicating the involvement of exTTF-SH molecular orbitals in conduction during this process (**Fig. S14**). Similarly, under negative bias, the current of the Au–S–C_{60}//SLG junction also shows a temperature-dependent decrease (**Fig. S15**). In contrast, the control Au-SC_{18}//SLG exhibits temperature-independent current characteristics of tunneling conduction (**Fig. S16b**). This demonstrates the influence of molecular orbital participation on the molecular junction within the two-terminal molecular junctions of Au-SAMs//SLG.

b) In **Section S4.4 Control experiments for molecular transistors**, we performed control experiments using junctions Au-SC_{18}//SLG with frontier orbitals energetically-distant (>2 eV) from the Fermi level. These unfunctionalized junctions exhibited a very small ON/OFF ratio of ~10 (**Fig. S23**), two orders of magnitude below that of the functional molecule, and similar in size to previously reported alkanethiolate SAMs (Chuancheng Jia et al., Sci. Adv. 2018, 4, eaat8237).

c) Regarding the blank Au//SLG junction in the absence of SAMs, the output characteristics exhibit linear I_{ds}-V_{ds} behavior, suggesting the formation of just an ohmic contact at the Au-SLG interface. Transfer characteristics show a negligible, background ON/OFF ratio of ~5 (**Fig.S24**).

These measured extremely small switching ratios in the control experiments with no or different SAM rule out graphene carrier-density tuning or gate-induced modification of SLG–molecule contact barriers as the cause of the observed large gate modulation with the functional molecules exTTF-SH and C_{60}-SH. The results in turn support the hypothesis that ionic-liquid-gated electric-field penetration through SLG enables modulation of the molecular frontier orbitals of exTTF-SH (HOMO transport) and C_{60}-SH (LUMO transport).

Changes made to the manuscript:

Page 7, Line 140-142: For comparison, we tested the electrical characteristics of the Au-SC_{18}//SLG junction, which exhibited a symmetrical current-voltage curve and current independent of temperature, consistent with tunnelling conduction (Fig.S16).

Page 10, Line 192-195: As a negative control, SC_{18} (1-octadecanethiol) with frontier orbitals energetically-distant (>2 eV) from the Fermi level showed extremely poor ON/OFF transistor ratios around 10, comparable to that of the SAM-less devices (~5) (Fig.S23, see also SAM-less devices in Fig.S24).[37]

Changes made to the supporting information:

Page 27, Line 298-301: Temperature-dependent measurements were carried out on Au-S-exTTF//SLG two-terminal junctions (Fig.S14), Au-S-C_{60}//SLG two-terminal junctions (Fig.S15) and Au-SC18//SLG two-terminal junctions (Fig.S16), to demonstrate the respective charge transport mechanisms for the two molecular junctions.

Page 28, Line 323-325:

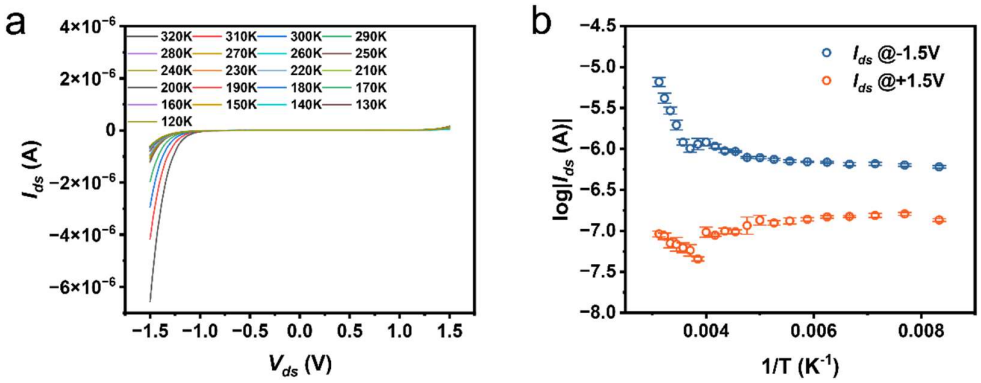

Figure S15. Temperature-dependent measurements I_{ds}-V_{ds} of two-terminal Au-S-C_{60}//SLG junctions. (a) Plots of current in linear scale versus bias. (b) log|I_{ds}| under different temperatures at V_{ds} = ± 1.5 V.

2. The electrical performance of the reported devices relies critically on the structural integrity, coverage, and ordering of the self-assembled monolayer (SAM) confined inside the micropores. However, the current manuscript provides very limited direct evidence for the quality of the molecular junction. The vertical gap thickness is inferred primarily from a single high-resolution TEM image showing an apparent ~1.5 nm separation, which may also contain contributions from residual oxide, contamination, or voids, and therefore cannot unambiguously confirm the presence of a well-formed, densely packed SAM. Please provide

additional and more direct characterization of the SAM, such as X-ray photoelectron spectroscopy, ellipsometry, infrared reflection–absorption spectroscopy (IRRAS), or contact angle measurements, to verify thiol anchoring, molecular coverage, and monolayer thickness.

Response: We thank the referee for raising the important point regarding the quality of the SAMs. It has been well established in the literature that the use of aluminum oxide pores to confine SAM growth does not compromise their formation (T. Lee et al, Nanotechnology, 2007, 18, 315204.; Bo W. Laursen et al, Adv. Mater., 2012, 24, 1333-1339.; C. A. Nijhuis et al, Adv. Funct. Mater., 2019, 29, 1904452.). In line with this, we screened various assembly solvents on gold-evaporated silicon wafers and characterized the resulting SAMs by XPS.

As detailed in **Section S3.3 Photoelectron spectroscopy**, we employed both XPS and UPS to analyze the SAMs. The S 2*p* results are the most important evidence to verify the quality of the SAMs (Nijhuis, C. A. et al, J. Am. Chem. Soc., 2014, 136, 1982-1991). In our results, the S 2*p* doublet at a binding energy of ~162.0 eV confirms thiolate anchoring through covalent Au–S bonds to the bottom gold electrodes. For the Au–S–exTTF SAM, an additional S 2*p* doublet at 163.5 eV with higher intensity indicates that the thiophene groups are located at the top of the monolayers (**Fig. S10**). The clean, well-resolved S 2*p* peaks are consistent with the formation of densely packed, well-ordered, upright monolayers in the junction region.

The thickness and relative surface coverage of the self-assembled monolayers (SAMs) were determined using X-ray photoelectron spectroscopy (XPS), following literature protocols (Yuan Li et al, Sci. Adv.,2023, 9, eadh3412). The resulting molecular lengths were consistent with the thickness values obtained from ellipsometry measurements. The calculated coverage approached full monolayer formation, indicating the high quality of the SAMs (**Table S4**). In addition, water contact angle measurements were performed to verify the surface modification by the different SAMs, confirming significant changes in wettability due to the functionalization of the gold surface (**Table S5**).

Changes made to the manuscript:

Page 6, Line 113-116: The chemical design of the HOMO- and LUMO-type molecular junctions are shown in Fig.1d. We characterized the growth quality of the self-assembled layer using XPS. The clean, well-resolved S 2*p* peaks are consistent with the formation of densely packed, well-ordered, upright monolayers in the junction region (Fig. S10).

Changes made to the supporting information:

Page 19-20, Line 221-238: The thickness and surface coverage of the monolayers can be calculated by

$$\frac{I_{C(1s)}}{I_{Au(4f)}} = k\frac{1 - e^{-d_C/\lambda_C}}{e^{-d_{CS}/\lambda_{Au}}}$$

where I is the integrated peak area, λ_C is the escape depth of C 1s photoelectrons through the carbon layer, λ_{Au} is the escape depth of the Au 4f photoelectrons through the thiolate layer, d_C is the thickness of the carbon layer, and d_{CS} is the thickness of the thiolate layer, and k is an instrument-specific constant. To calibrate the instrument, the C_{1s}/Au_{4f} intensity ratios of all samples were calculated and compared with the corresponding ratio for SC_{18} -SAMs of known thickness [21] to obtain the thickness of all samples.

Once the thickness d was obtained, the surface coverage could be derived. The relative surface coverage Γ_{SAM} was estimated by comparing the attenuated Au 4f signals of SAMs with different anchoring groups, using the expression:

$$I_{0,Au} = \frac{I_{Au}}{e^{-d/\lambda}}$$

Here, $I_{0,Au}$ denotes the hypothetical Au 4f signal in the absence of attenuation by the SAM. The measured surface coverage of SC18 on Au has been reported as 6.94×10^{-10} mol cm^{-2} [21]. Therefore, by comparing the $I_{0,Au}$ values of all SAMs with that of SC_{18} on Au, the corresponding Γ_{SAM} values for the SAMs in this study were estimated.

Page 24, Line 271-275: Section S3.5 Additional characterization of SAMs

Table S4. Thickness and coverage of SAMs

SAMs	Thickness (Å) (ellipsometer)	Thickness (Å) (XPS)	Surface coverage (1×10^{-10} mol/cm^2)
exTTF-SH	24.4±2.1	23.9	6.74
C_{60}-SH	25.0±0.6	24.6	5.29
Fc-SH	24.0±1.3	23.2	6.82
PDI-SH	23.1±0.8	23.3	6.49
C18-SH[21]		23.3	6.94

Table S5. Water contact angle of SAMs

SAMs	Water contact angle (°)

exTTF-SH	69.2±1.8
C_{60}-SH	94.1±1.1
Fc-SH	77.8±1.3
PDI-SH	76.3±1.5

3. Furthermore, statistical information on the micropore geometry (diameter, depth, and residual dielectric thickness), obtained from cross-sectional SEM, AFM, or multiple TEM images, is necessary to establish the uniformity of the vertical junctions and to rationalize device-to-device current variations.

Response: We appreciate the referee's comments on our device fabrication. In **Section S3.1 Device fabrication**, we characterized the Al_2O_3 micropores within the device and the overlying graphene. Figure S6b shows an optical microscopy image of a micropore. AFM measurements revealed a pore height of 30 nm (Fig. S6c) and a gold surface roughness of 1.0 nm (Fig. S6d). The fabrication of the 5.0 μm diameter micropores used an AZ601-46cp-based photoresist process. After development, residual photoresist was removed with oxygen plasma. The alumina was then etched for 30 seconds using BOE (28 ml of 49% HF added to 170 ml of 40% NH_4F solution). This wet etching, with an over-etch time exceeding 50%, ensured complete removal of the dielectric layer from the gold surface. EDS characterization showed no or only background-level Al signal within the pores (Fig. S6f), and the consistent roughness values measured from AFM confirmed sufficient alumina etching.

Process variations were statistically analyzed. AFM measurements of 38 pores across 9 devices showed an area distribution of 21.78 ± 1.02 μm², a deviation of 4.7% (Fig. S6e), indicating minimal impact on current distribution accuracy. The Al_2O_3 height, deposited by ALD, was 32.80 ± 3.48 nm (~10.6% deviation). Both AFM and TEM revealed a >100 nm gentle slope at the pore edges from wet etching. This makes the exact pore height non-critical and allows graphene to form complete, continuous coverage.

Crucially, regarding reported switching performance: Any dimensional variations do not affect the switching ratio. This is because the ratio is calculated from the on- and off-state currents within a single measurement curve, where the pore geometry is constant.

Changes made to the manuscript:

Page 5, Line 81-83: EDS characterization revealed no aluminium oxide residue on the gold

surface within the pores. AFM validation confirmed the uniformity of pore area, with the gold roughness within the pores being consistently ~1 nm (Fig. S6).

Changes made to the supporting information:

Page 15, Line 174-183: Process variations were subjected to statistical analysis. AFM measurements of 38 pores across 9 devices yielded an area distribution of 21.78 ± 1.02 μm², corresponding to a 4.7% variation (Fig. S6e), which indicates a minimal impact on the accuracy of current distribution. Both AFM and TEM revealed a gentle slope exceeding 100 nm at the pore edges resulting from wet etching. This feature renders the exact pore height non-critical and enables the graphene to form complete, continuous coverage. EDS characterization showed no or only background-level Al signal inside the pores (Fig. S6f). Consistent surface roughness measurements from AFM further confirmed sufficient etching of the alumina.

Page 17, Line 189-194:

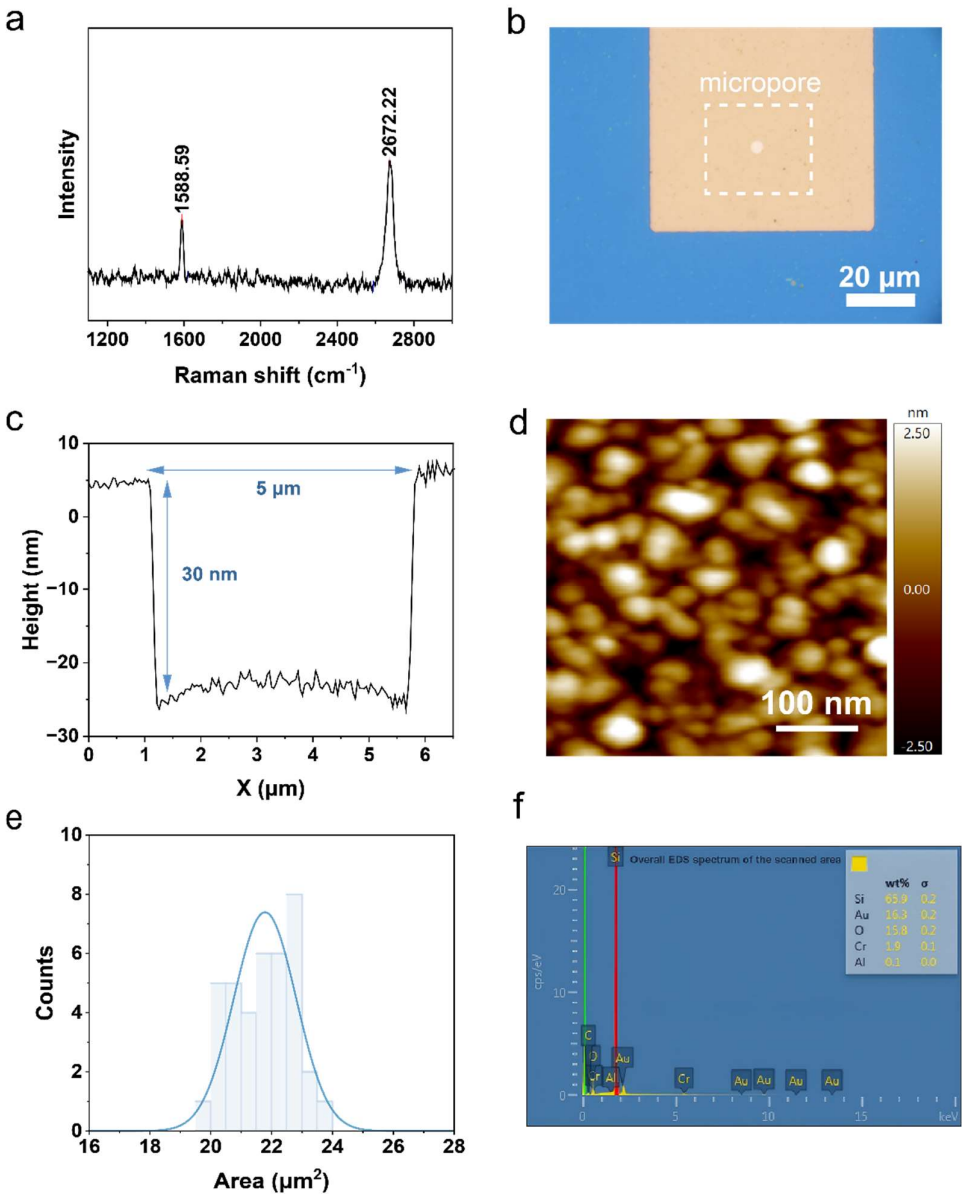

Figure S6. a. Raman spectrum of single-layer graphene. b. Optical image of Al_2O_3 micropore on Au pad. c. Section profile of Al_2O_3 micropore recorded by AFM. d. AFM image of Au substrate with surface roughness of 1.0 nm. e. The area of Al_2O_3 pores obtained by AFM exhibits a normal distribution with a mean of 21.78 ± 1.02 μm². f. Overall EDS spectrum within the Al_2O_3 pore show an elemental statistical proportion of 0.1 wt%, consistent with the background, while the non-etched area exhibits 2 wt%.

4. Additionally, since multiple molecular species (exTTF, C60, Fc, and PDI derivatives) are employed, a comparative discussion of their respective SAM quality and packing behavior

would significantly strengthen the structural interpretation of the electrical results.

Response: We appreciate the referee's attention to the variety of molecular systems used in our study. Molecular junctions developed based on SAMs require consideration not only of the influence of their electronic structure on electrical properties but also of the role of supramolecular structures. Intermolecular interactions affect the density of SAMs, thereby significantly impacting charge transport (Thompson & Nijhuis Acc. Chem. Res., 2016, 49, 2061). As observed in our work, the quality and packing behavior of each type of molecular SAM significantly influences the electrical performance, particularly the off-state current and its stability. Since LUMO-type molecules typically possess extensive conjugated structures, they exhibit poor solubility and aggregation regularity, hindering the growth of dense, ordered SAMs. For instance, in LUMO-type molecules with the same backbone but one without side chains, reduced solubility and lower packing density led to a markedly lower switching ratio (**Figure S21**).

For the four molecules presented in this paper, we optimized both the molecular backbone and the solvent system for SAM growth. This enabled the formation of well-packed monolayers, which yielded relatively stable currents and low off-state currents. Specifically, for exTTF and Fc, the rigid phenyl-vinylbenzene backbone promoted tightly ordered stacking and minimized defects. For C_{60} and PDI, whose functional groups exhibit low solubility, high-density SAMs could not be achieved directly; therefore, alkyl backbones with side chains were introduced to obtain well-stacked monolayers. Consequently, for these four systems, we attribute the differences in electrical properties primarily to the energy-level alignment between the top functional groups and graphene, as well as to variations in the electronic coupling strength between those functional groups and graphene.

Changes made to the manuscript:

Page 10, Line 196-200: The quality and supramolecular structure of SAMs significantly influence their electrical properties, particularly the off-state current and its stability (Section S4.3). For the four systems we report, optimization of the scaffold structure and SAM growth conditions resulted in all cases in well-packed structures (Section S3). Therefore, the relative alignment between the frontier molecular orbitals and the E_F of the SLG is the determining factor for the distinct behaviors.

Changes made to the supporting information:

Page 33, Line 360-376: Section S4.3 The Influence of Supramolecular Structures on Molecular Transistors

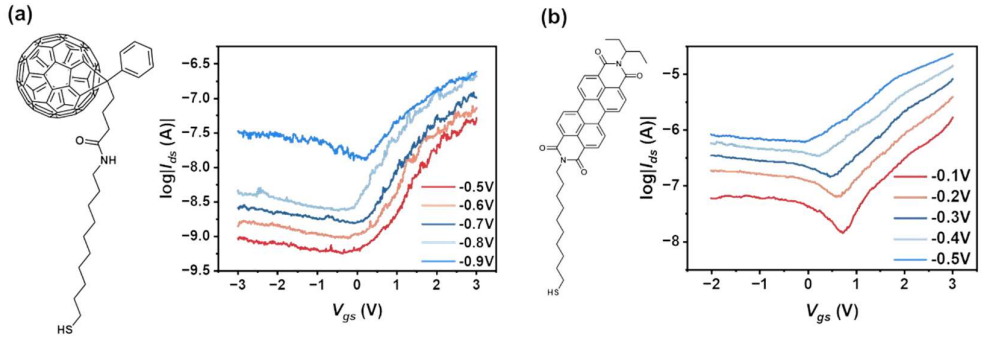

Figure S21. a. Structural diagram of C_{60} molecule without side chains and its measured FET transfer curve diagram. b. Structural diagram of PDI molecule without side chains and its measured FET transfer curve diagram.

5. The manuscript claims wafer-scale integration of approximately 8000 molecular transistors on a 2-inch wafer with an impressive reported yield of 94.8%; however, the definition of "yield" adopted here is overly permissive and does not adequately reflect true functional performance. At present, devices are classified as "working" primarily based on the observation of nonlinear I–V characteristics, which essentially confirms that the junctions are not electrically shorted but does not guarantee transistor-like switching behavior. A more rigorous distinction should be made between physical electrical yield (non-shorted junctions) and functional transistor yield defined by a minimum ON/OFF ratio, subthreshold slope, or transconductance.

Response: We appreciate the referee's point regarding a more careful classification of junctions in terms of both physical yield (non-shorted junctions) and functional transistor yield (transistor vs. non-functional). In response, we performed further data processing and analysis, using the ON/OFF ratio as a metric for classifying functional transistor behavior while incorporating calculations and statistics related to subthreshold swing. (**Figure S30**) From the ON/OFF analysis, transistors with log(ON/OFF) > 3.0 were classified as functional, as values below this threshold deviate significantly from the fitted normal distribution. This switching-ratio criterion gives a functional yield of 84.0%. In parallel, we extracted the subthreshold swing for all transfer curves. To reduce the influence of capacitive spikes on SS extraction, a wider fitting window of 0.375 V was applied. The resulting SS distribution is 767 ± 354 mV/dec. Using

SS < 1000 mV/dec as the functional threshold, the corresponding yield is 77.6%.

Thus, among the originally identified "working" transistors, nearly 80% demonstrate ultra-robust transistor characteristics. Combining both metrics, we confirm a conservative functional transistor yield of 73% (94.8% × 77%) for our devices.

Changes made to the manuscript:

Page 17, Line 317-318: Correspondingly, the yield of functional field-effect transistors defined by on-off ratio and subthreshold swing is 73% (94.8% × 77%) (Fig. S30).

Changes made to the supporting information:

Page 39-40, Line 446-460: We performed further data processing and analysis, using the ON/OFF ratio as a metric for classifying functional transistor behavior while incorporating calculations and statistics related to subthreshold swing. (Figure.S30) From the ON/OFF analysis, transistors with log(ON/OFF) > 3.0 were classified as functional, as values below this threshold deviate significantly from the fitted normal distribution. This switching-ratio criterion gives a functional yield of 84.0%. In parallel, we extracted the subthreshold swing for all transfer curves. To reduce the influence of capacitive spikes on SS extraction, a wider fitting window of 0.375 V was applied. The resulting SS distribution is 767 ± 354 mV/dec. Using SS < 1000 mV/dec as the functional threshold, the corresponding yield is 77.6%. Thus, among the originally identified "working" transistors, nearly 77% demonstrate ultrarobust transistor characteristics. Given that the yield of originally identified working transistors is 94.8%, the combined conservative functional transistor yield is therefore 94.8% × 77% = 73%. Combining both metrics, we confirm a conservative functional transistor yield of 73% for our devices.

Page 43, Line 487-490:

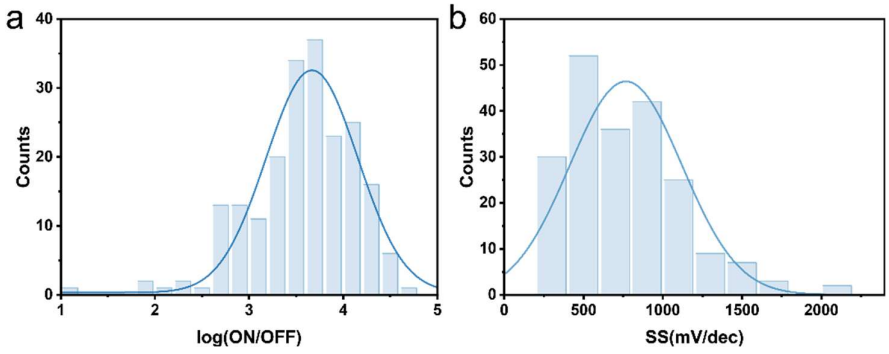

Figure S30. a. Distribution of ON/OFF ratios corresponding to transfer characteristic curves (V_(ds) = 0.1 V) of 200 randomly selected HOMO-type molecular transistors. ON/OFF =

4,660; σ log(ON/OFF) = 0.49. b. Subthreshold swing distribution for 200 randomly selected HOMO-type molecular transistors, showing 767 ± 354 mV/dec.

6. In addition, the statistical analysis presented in Fig. 5e is internally inconsistent, where the reported average value of log (ON/OFF) and its standard deviation appear numerically implausible and require careful re-evaluation and clarification. The current statistics also seem to be obtained from a limited subset of devices on a single wafer. To support the strong claims of wafer-scale manufacturability, the authors should present spatially resolved ON/OFF maps across the entire wafer and, ideally, include wafer-to-wafer reproducibility over multiple fabrication runs. Without such rigorous statistical treatment, the claims of high-yield, large-scale integration remain insufficiently substantiated.

Response: For the results in **Figure 5e**, we have corrected the specific numerical values and standard deviations obtained. The correct results should be: ON/OFF = 4,660 (log(ON/OFF) = 3.67) with $\sigma_{log(ON/OFF)}$ = 0.49. This error occurred during the conversion of logarithmic results to linear results. We apologize for this error, and we thank the reviewer for catching it.

Changes made to the manuscript:

Page 17, Line 326-328: The log(ON/OFF) values exhibit a tight normal distribution. After conversion to exponential form, the mean is 4660, and the standard deviation of the normal distribution of the logarithmic values is 0.49.

Further response: We thank the referee for raising the need for greater clarity in our reporting. In **Section S4.6 Electrical measurements of integrated molecular transistors**, we noted that the results were obtained from four 2-inch wafers fabricated in parallel across two batches. During electrical testing, measurements were taken from multiple distinct regions on these wafers, with each region containing 36 transistors and approximately 10 points measured per region. The reported dataset is based on independent measurements across roughly 17 different regions—one of which involved testing all 36 transistors in that region. We performed statistical analysis of the ON/OFF ratios separately for each device. The results show that the distribution of ON/OFF ratios remains consistent across devices #1 to #4 (**Figure S26**), indicating that our data—drawn from a large number of devices across multiple wafers—exhibits highly repeatable statistical behaviour suitable for mass fabrication.

We apologize for the temporary inability to provide spatially resolved ON/OFF distribution maps on the wafer, as the specific locations of the test regions were not systematically recorded during preliminary measurements, and device fabrication and testing require a significant amount of time well beyond the time of the review cycle. This issue will be addressed in subsequent studies. Additionally, we believe that the yield in the device edge regions may be lower, primarily due to challenges in the graphene transfer process—specifically, the edge regions are more susceptible to contamination and breakage during the wet transfer process.

Changes made to the manuscript:

Page 17, Line 324-326: The measured transfer characteristics of 200 randomly-selected HOMO-type molecular transistors (Fig.5d, Fig.S28-30) showed consistent ideal switching behavior across 17 regions in four distinct devices.

Changes made to the supporting information:

Page 39, Line 435-443: During electrical testing, measurements were taken from multiple distinct regions on these wafers, with each region containing 36 transistors and approximately 10 points measured per region. The reported dataset is based on independent measurements across roughly 17 different regions—one of which involved testing all 36 transistors in that region. We performed statistical analysis of the ON/OFF ratios separately for each device. The results show that the distribution of ON/OFF ratios remains consistent across devices #1 to #4 (Figure.S26), indicating that our data—drawn from a large number of devices across multiple wafers—exhibits highly repeatable statistical behaviour suitable for mass fabrication.

Page 40, Line 466-472:

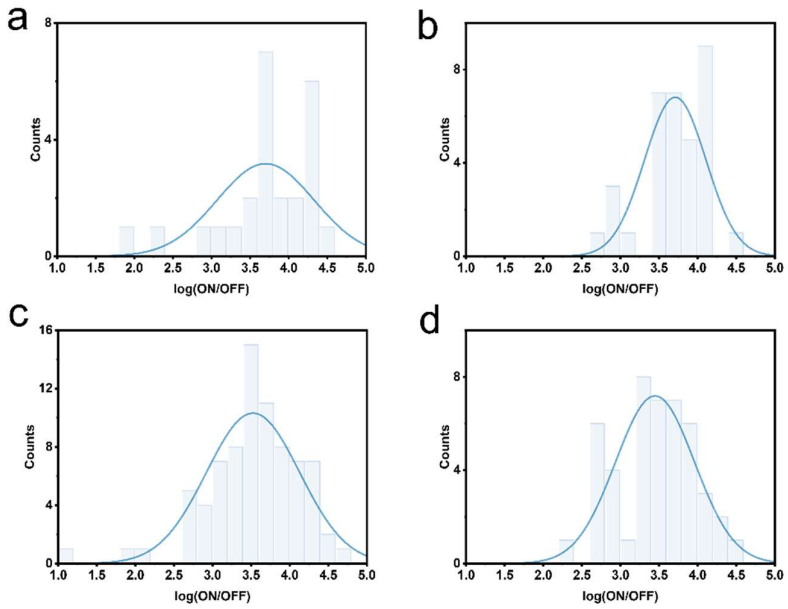

Figure S26. a. Device #1 measured ON/OFF ratio distribution of the transfer characteristic curve, yielding a distribution result of log(ON/OFF) = 3.70 σlog(ON/OFF) = 0.63. a. Device #2 measured ON/OFF ratio distribution, yielding a distribution result of log(ON/OFF) = 3.71 σlog(ON/OFF) = 0.40. c. Device #3 measured ON/OFF ratio distribution, yielding a distribution result of log(ON/OFF) = 3.52 σlog(ON/OFF) = 0.60. d. Device #4 measured ON/OFF ratio distribution, yielding a distribution result of log(ON/OFF) = 3.44 σlog(ON/OFF) = 0.51.

Minor revision:

1. Several minor issues regarding presentation, notation, and clarity should also be addressed to improve the overall readability and accuracy of the manuscript. For example, there are evident inconsistencies in figure numbering and cross-referencing, particularly in the wafer-scale integration section where the figure labeled as “Figure 4” should correspond to “Figure 5,” and multiple internal references appear inconsistent.

We apologize for these errors and have corrected them all in the revised text which is now error free of all typos or inconsistencies in notation and numbering.

Reviewer #4 (Remarks to the Author):

This manuscript reports high-performance vertical SAM-based molecular transistors using an ionic-liquid electrochemical gate. The authors show that drain-current modulation is governed by molecular-orbital/graphene-Fermi-level alignment, enabling a clear classification of HOMO- and LUMO-type molecular transistors with an intuitive p/n-type analogy. Moreover, xthe work demonstrates ON/OFF ratios >10^4 at and above room temperature, >100,000-cycle stability, and >90% fabrication yield, together with dense arrays on a 2-inch wafer and functional logic-gate demonstrations. Overall, the technological achievements presented here are impressive. I recommend minor revision before acceptance of Nature Communications, while some concerns regarding the theoretical interpretation of the transport mechanism and the rigorousness of the integration demonstration have been addressed.

Response: We appreciate the expert reviewer's summary of the results and presented mechanism, and for the encouragement regarding the technological significance of the data. We are grateful for the recommendation to publish following minor revision. All the referee's concerns regarding the theoretical interpretation of the transport mechanism and the rigorousness of the integration demonstration have been fully addressed as described below.

1. The theoretical modeling appears to predict an opposite trend compared to the experimental data, which raises concerns regarding the validity of the proposed transport mechanism. Specifically, the calculated transmission spectra and current-voltage curves (Fig.2c-2d) suggest that the Au-S-exTTF//SLG junction should exhibit higher conductivity than Au-S-C60//SLG system. However, the experimental results demonstrate significantly higher current densities for the C60-based junctions. This qualitative discrepancy suggests that the theoretical model (likely based on a single-molecule junction approximation) may not be representative of the actual experimental setup. Could this mismatch be attributed to intermolecular interactions that are absent in the single-molecule calculation? The authors should provide a detailed discussion or additional calculations to reconcile this contradiction.

Response: We appreciate the reviewer's very relevant comment about the calculation. Indeed, the currents and transmission functions predicted by Tight Binding (DFTB) calculations are much lower for Au-S-C_{60} than Au-S-exTTF, and this is at odds with the experimental data. To check this, both systems were calculated using DFT with SIESTA software. The results, shown in Supporting Information (Figure S35), were similar to those obtained using DFTB, showing

that the level of accuracy of the method used does not change the predicted ranking of the molecules in terms of conductivity. For this reason, we agree with the reviewer that the discrepancy likely stems from the absence of molecular packing in the model. This is reflected in the position of the HOMO and LUMO displayed in Figure 1e. The predicted HOMO of exTTF is closer to the Fermi level than experimentally measured, and the predicted C_{60} LUMO is further from the Fermi level than experimentally measured. The experimental data, however, were obtained from the SAM. Unfortunately, modelling the supramolecular assembly of a sizeable array of molecules, representative of a SAM, is currently unfeasible for quantum methods as the number of atoms would exceed the capabilities of electron transport algorithms. Additionally, the experimental systems are transistors, while the computational models are simple junctions. No current implementation of multiple-electrode transport calculation enables accounting for the field effect induced by the gate. The absence of this effect also contributes to the discrepancy. The most important result of the modelling is that, in line with the interpretation of experimental results, the relative position with respect to the Fermi level of gold of the HOMO for p-type systems and of the LUMO for n-type governs the electron transport mechanism, and therefore the output current.

Changes made to the manuscript:

Page 8, Line 153-154: For further discussion of the modelling results and control calculations see Supporting Information page 45.

Changes made to the supporting information:

Page 47, Line 519-541: The DFTB modelling-predicted Au-S-C_{60} current is much lower than Au-S-exTTF, contrary to the experimental data. To check the cause of this discrepancy, additional calculations were carried out using full DFT with SIESTA[34, 35] and its associate transport software TBTrans[36, 37]. The GGA functional PBE[38] was used with a double-zeta basis set and optimized norm-conserving Vanderbilt pseudopotentials[39, 40] provided in the PseudoDojo library[41-43]. The DFT results, shown in Figure S35, are similar in amplitude to those obtained using DFTB. This shows that the computational method does not change the predicted ranking of the molecules in terms conductivity. Thus, this discrepancy likely stems from the absence of supramolecular packing in the model.[44, 45] This is reflected in the position of the HOMO and LUMO displayed in Figure 1e. The predicted HOMO of exTTF is closer to the Fermi level than experimentally measured, and the predicted C_{60} LUMO is further from the Fermi level than experimentally measured. The experimental data, however, were obtained from SAM, not idealised single molecule, devices. Furthermore, the computational

models are simple junctions, not transistors, which cannot be yet modelled with existing charge transport algorithms. The absence of the field effect may also contribute to the discrepancy between experiment and theory. However, our model shows, in line with the interpretation of experimental results, that the relative position with respect to the Fermi level of gold of the HOMO for p-type systems and of the LUMO for n-type governs the electron transport mechanism, and therefore the output current. The model thus predict that it is possible for gate voltage V_{gs} to shift the positions of the molecular orbitals and regulate the channel conductance, which guides the interpretation of the experimental electrical measurements.

2. Another concern is, according to the calculated transmission spectrum for the Au-S-exTTF//SLG junction, the transport characteristics are expected to exhibit a V-shaped (ambipolar) evolution or a non-monotonic trend as the gate voltage shifts the Fermi level across the transmission features.

Response: We thank the reviewer for this detailed analysis of the calculated transmission functions. These transmission functions were obtained using the two-electrode model for which no gate was present. Therefore, the model is limited in its ability to map the fine details of the shape the experimentally measured I-V curves take under the polarizing effect of a gate. We note that, as shown, in **Figure 2d**, the source-drain currents do display a non-monotonic behaviour, similar to the one observed experimentally, and consistent with the transmission functions. The distinct asymmetry of the computed I-V plots is also consistent with the transmission function. Figure S35 shows results obtained using DFT (PBE/DZVP) with SIESTA software, for the same two-electrode model. The transmission functions present a higher level of symmetry around the source-drain 0 V bias. This, in turns, leads to I-V curves with the distinct V-shape. The asymmetry observed in the plots in Figure 2d is thus considered an artefact of the Tight Binding method.

Changes made to the manuscript:

Page 8, Line 154-159: Additionally, the computational models caputure the non-monitonic behaviour of the current as a function of the source-drain bias.[46-48] Both the DFT and DFTB models exhibit the characteristic V-shape, with the DFTB model overestimating the asymmetry observed experimentally, while the DFT model underestimates it, which may be due to model limtations (absence of gate and supramolecular packing); for more discussion see Supporting Information page 45.

3. The demonstration of wafer-scale integration (Fig. 5) is arguably the most significant breakthrough of this work. However, in Figure 4, the illustration and optical images of the HOMO- and LUMO-type transistors used to create the NOT gate appear to stem from separate regions or discrete devices that were potentially wired together externally, rather than being integrated side-by-side in a compact circuit layout. To prove the robustness of their fabrication process and the feasibility of true integration, the authors should demonstrate the logic gates (e.g., the NOT gate) directly within the wafer-scale array shown in Fig. 5. Demonstrating adjacent, lithographically defined p-type and n-type devices functioning as a logic unit on the same wafer coordinates would significantly strengthen the claim of large-scale integration.

Response: We thank the referee for acknowledging the significant breakthrough of the wafer-scale integration (Fig. 5). In **Section S3.5 On-chip combination of HOMO- and LUMO-type molecular junctions**, we describe our fabrication process. We employed a simple method to fabricate on-chip combinations of HOMO- and LUMO-type molecular junctions to realize a NOT gate. Half of the as-fabricated patch was immersed in exTTF-SH solution for one day and washed with the corresponding solvent to form HOMO-type SAMs. Then we reversed the patch to immerse the other half in C_{60}-SH solution to form LUMO-type SAMs on the same patch. In this way, the two functional regions were integrated through sequential immersion in different molecular solutions. These combined molecular junction devices are designed primarily to demonstrate how different types of molecular transistors can enable logic functions without external resistors, thereby simplifying circuit design.

Notably, the controlled growth of distinct types of self-assembled monolayers (SAMs) in adjacent regions on a single wafer remains a persistent challenge technically. While our previously developed microchannel approach using polydimethylsiloxane (PDMS) allowed different areas of a device to form unique SAMs with selected molecules (Y. Li et al., Adv. Mater. 2024, 36, 2406456.), this method faces limitations in channel dimensions, pattern density, and, critically, compatibility with standard CMOS processes (Chiechi, R.C et al., Nat. Commun. 2022, 13, 2312). As a result, it is not suitable for the large-scale, wafer-level array integration demonstrated in Figure 5.

Thanks to the reviewer's inspiring and motivating suggestion, the technique presented in this work opens new pathways for integrating diverse SAMs on the same substrate. By sequentially etching a subset of channels, growing the corresponding SAM, depositing and patterning graphene, and then repeating these steps for another set of channels with a different SAM, on-

wafer integration of multiple molecular layers becomes feasible. Nevertheless, several challenges must be addressed, including the uncertain influence of multilayer graphene on gate control performance and potential yield reduction due to the increased number of fabrication steps. These aspects will be the focus of our subsequent work to further advance this technology.

Changes made to the manuscript:

Page 15, Line 294-297: We accomplished this by grouping all junctions for each molecular type at one end of the device, then selectively immersing each end in its corresponding molecular solution to grow the respective SAMs, as detailed in the Supporting Information Section S3.5.

4. The authors evaluate the charge transport mechanism (via temperature-dependent measurements) for exTTF-SH junctions at a fixed bias of Vds = +0.5 V. However, I note that Figures 4a-b do not appear to present the data at this specific voltage range, creating a disconnect between the device characterization and the mechanism analysis. Since the Au-S-exTTF//SLG junction is structurally and electronically asymmetric, it is scientifically unsound to assume that the transport mechanism at derived at Vds = 0.5V applies to the negative bias regime in Fig.4a-b.

Response: We sincerely appreciate the reviewer's suggestion for the choice of dataset for the mechanism discussions. We have retested the temperature dependence obtained at V_{ds} = -0.5 V and found the results are consistent with those previously obtained at +0.5 V. As demonstrated in **Figure. S18**, we observed that the variations in V_{ds} exert a minor influence on the switching ratio of the molecular field-effect transistor, with both conditions exhibiting similar switching phenomena, albeit with differences in current magnitude. However, further analysis of the temperature-dependent data revealed that the activation energy for exTTF under negative bias (126 meV) is higher than under positive bias (61 meV). We attribute this difference to the SAM–electrode interaction: under negative bias, the coupling strength between exTTF and graphene differs from that under positive bias, consequently leading to the observed variation in activation energy. We infer this difference may come from the Coulombic interactions between SLG and the positively charged (oxidized) exTTF moieties: attractive at negative bias and repulsion at positive bias.

Changes made to the manuscript:

Page 13, Line 239-244: To further explain the similar transmission characteristic behavior under both positive and negative V_{ds} conditions, we also performed temperature-dependent measurements on the transmission characteristic curves with V_{ds} fixed at +0.5 V. The results indicate that hopping behavior is observed under negative gate voltage, while tunneling is exhibited under positive gate voltage, consistent with the behavior under positive bias (Fig.S18).

Changes made to the supporting information:

Page 30 Line 337-341: We also tested the temperature dependence at $V_{ds} = -0.5$ V and found the results to be largely consistent with those previously obtained at $+0.5$ V. As shown in Figure S18, variations in V_{ds} have only a minor effect on the switching ratio of the molecular field-effect transistor. Similar switching behavior is observed under both bias conditions, although the absolute current levels differ.

Page 30, Line 349-351:

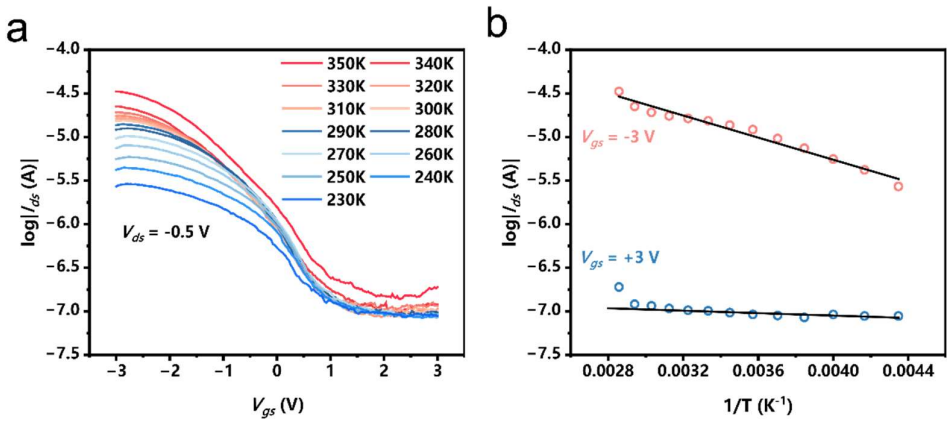

Figure S18. a. The temperature-dependent transfer characteristics for HOMO-type transistors at V_{ds} = -0.5 V. b. corresponding Arrhenius plots of log|I_{ds}| at ON and OFF state.

Reviewer #5 (Remarks to the Author):

This works is a nice effort towards the implementation of robust molecular transistors. The work encompasses the most important aspects enabling molecular transistors applications such as stability and scalability, which are today limiting their real world applications. The transistor operation relies on the well-known principle allowing switching molecular transport regime between off-resonant tunnelling and 1-level hopping via a redox functional group engineered into the active molecular backbone. The engineering approach to stabilise the active molecular layer into a micrometre size pore feature using a single-layer graphene top contact is clever and brings advantages towards the scalability of the process and integration in current microfab methods. All in all, I feel this will be a nice contribution to the field with wide impact on the microelectronics community.

Response: We express our sincere gratitude to the reviewer for the positive assessment of our work and for recognizing it as a "nice contribution to the field with wide impact." We also thank the reviewer for the thoughtful and constructive queries, which have helped us to significantly improve the clarity and depth of our manuscript. Below, we provide a point-by-point response to all the comments.

Prior to publication of the work, I do have a few queries and clarifications for the authors I am listing below:

- I find the concept of SAM ill-defined here. There is no way molecular structures like the ones used in this work will form a nice compact monolayer as it seems to be suggested in different passages of the manuscript. The HRTEM images showing a small gap are no proof of the structural integrity of the molecular layer, which will surely bear plenty of defects, vacancies, etc. To be fair, I think a small paragraph stating how this can affect device operation and/or they can be overcome thanks to the device structure needs to be incorporated.

Response: We thank the reviewer for raising this important point regarding the structural integrity of the self-assembled monolayer (SAM). We apologize for not sufficiently detailing our efforts to ensure a high-quality monolayer in the initial manuscript. As demonstrated in previous studies, the use of dielectric (e.g., alumina) nanopores is a well-established method for fabricating molecular junctions (T. Lee et al, Nanotechnology, 2007, 18, 315204.; Bo W. Laursen et al, Adv. Mater., 2012, 24, 1333-1339.; C. A. Nijhuis et al, Adv. Funct. Mater., 2019,

29, 1904452.), and it has been shown that this approach has a minimal adverse effect on the formation of monolayers.

In our device design, we optimized the device fabrication process to promote formation of the highest quality SAMs. This involved carefully controlling the evaporation parameters for the Cr/Au bottom electrode to achieve an ultra-smooth surface with an RMS roughness of approximately 1 nm. Subsequently, the fabrication of the alumina pore via ALD and wet etching ensures that the exposed gold surface within the pore is consistent with the as-deposited smooth surface, following established methodologies in the field.

Beyond substrate optimization, our primary strategy to obtain a compact monolayer focused on the molecular design itself: employing an appropriate molecular backbone, utilizing a robust thiol anchoring group, and optimizing the growth solvent conditions. To verify the quality of the SAMs, we performed comprehensive characterizations on planar, pore-free gold-on-silicon substrates. As shown in Supplementary Information Section 3.3 and 3.5, X-ray Photoelectron Spectroscopy (XPS) and Ultraviolet Photoelectron Spectroscopy (UPS) confirm the successful growth of high-quality molecular layers.

Regarding the SAMs grown within the pores, we acknowledge that Atomic Force Microscopy (AFM) cannot provide direct proof of molecular ordering at the monolayer level. However, AFM topography scans of the pores after SAM formation consistently showed a surface roughness of approximately 1 nm, both across 3 μm and 500 nm scan areas. This indicates a conformal coating without large-scale aggregation or defects. The only exception was the C60-based SAM, which exhibited a slightly higher roughness of ~1.7 nm. We attribute this to the larger molecular size of C60 and its tendency to arrange with vertical height fluctuations at high coverages.

The reviewer is absolutely correct there is no defect-free SAM in any large-area devices. This monolayer must naturally feature edge-defects and vacancies, and it is not our intention to give readers any impression that monolayers are defect-free. We have now added a discussion to the main text and supplementary information, explicitly stating that a poorly formed monolayer with significant defects would lead to degraded device performance (e.g., lower ON-OFF ratios, higher leakage currents, and larger device-to-device variability).

Changes made to the manuscript:

Page 10, Line 196-200: The quality and supramolecular structure of SAMs significantly influence their electrical properties, particularly the off-state current and its stability (Section S4.3). For the four systems we report, optimization of the scaffold structure and SAM growth

conditions resulted in all cases in well-packed structures (Section S3). Therefore, the relative alignment between the frontier molecular orbitals and the E_F of the SLG is the determining factor for the distinct behaviors.

Changes made to the supporting information:

Page 33, Line 360-376: Section S4.3 The Influence of Supramolecular Structures on Molecular Transistors

- Fig. 1e oversimplifies the electronic structure of the graphene layer. As part of the device manufacturing, the graphene is layer seems to be etched into some sort of nanoribbons which surely will increase the existing electronic gap of graphene. This would affect the observed transistor operation and should be incorporated as part of the discussion of results.

Response: We thank the reviewer for this comment. In our fabrication process for both individual and wafer-scale devices, the graphene layer is patterned into dimensions of 80 μm in length and 20 μm in width (or larger). These dimensions are several orders of magnitude larger than those of graphene nanoribbons, which typically necessitates patterning into nanoribbons with widths below 10-20 nm (Gustavo E. Scuseria et al, Nano Lett. 2006, 6, 12, 2748–2754). While we acknowledge that patterning can, in principle, introduce subtle edge effects that might influence the Fermi velocity or local carrier density, we have observed consistent device performance across numerous devices with varying patterned graphene sizes. Therefore, we are confident that for the length scales used in our study, the contribution of the patterned edges to the electronic structure is negligible and does not affect the core operating principle of the transistor.

Changes made to the manuscript:

Page 5, Line 83-86: After forming the Au-SAM//SLG junction (the SLG was patterned into tens-of-micrometer dimensions, well above the threshold for bandgap opening), an ionic liquid $[DEME]^+[TFSI]^-$ (N,N-diethyl-N-methyl-N-(2-methoxyethyl)ammonium bis(trifluoromethylsulfonyl)imide) was dropped on the SLG.

- The exponential portion of the intended Arrhenius plot in S14b needs explanation.

Response: We thank the reviewer for the opportunity to clarify this observation. The non-linear behavior of the Arrhenius plot in Figure S14b, showing a temperature-dependent (thermally activated) region at high temperatures and a temperature-independent (saturation) region at low temperatures, has been observed in other molecular devices. This effect was reported in early work by van der Zant et al. (Nano Lett., 2006, 6, 1031–1035.) and has been comprehensively explained in the framework of a single-level tunneling model. As detailed by Christian A. Nijhuis and colleagues in their 2016 paper ("A Single-Level Tunnel Model to Account for Electrical Transport through Single Molecule- and Self-Assembled Monolayer-based Junctions", Sci Rep, 2016, 6, 26517.), this behavior can be understood in terms of a broadening of the molecular energy level. At higher temperatures, internal molecular vibrations, excited by the increasing current as the system is brought closer to resonance, broaden the level width, leading to an activated transport process. As the temperature decreases further, this vibration-induced broadening freezes out, and the transport enters a quantum coherent regime where the current becomes temperature-independent. This plateau at low temperatures is a signature of coherent, off-resonant tunneling, consistent with our interpretation.

Changes made to the supporting information:

Page 27, Line 301-316: We have incorporated this discussion into the relevant section of the SI.

- The asymmetry of the IVs in Fig. 2a is hard to see considering the dispersion. This questions its role in the observed transistor effect. Is the asymmetry stronger at higher voltage biases?

We appreciate the reviewer's insightful question regarding the role of *IV* asymmetry. For the exTTF molecule shown in Figure 2a, the temperature-dependent transport measurements indicate that within the applied bias range of ±0.5 V, the junction operates within the single-level model, meaning the molecular energy level resides within the bias window defined by the Fermi levels of the two electrodes. Under this condition, significant rectification is not expected. We agree with the reviewer that at higher bias voltages, the asymmetry would likely become more pronounced as the level is pushed further into the bias window, but we expect that the higher bias voltages would also irreversibly damage the SAM.

- How is this poor asymmetry translated to the strong ON-OFF transistor behaviour?

Crucially, the strong ON-OFF transistor behavior observed in our devices is not primarily governed by the asymmetry in the two-terminal *IV* characteristics. Instead, it is a direct result

of gate-voltage-controlled energy level alignment. Our temperature-dependent transfer characteristic measurements reveal that at $V_g = 0$ V and negative gate voltages, the current is temperature-dependent, indicating a hopping transport regime (ON state). At $V_g = +3$ V, the current becomes temperature-independent, signifying a transition to a tunneling regime (OFF state) where the molecular level is gated out of the resonance window. Therefore, the key to achieving a high ON-OFF ratio lies in the ability of the gate to shift the molecular energy level relative to the electrode Fermi levels, which is contingent on two factors: (1) the intrinsic energy level of the functional group being close to the electrodes' Fermi level, and (2) an appropriate coupling strength between the molecule and the graphene electrode. This gate-controlled switching is a separate phenomenon from bias-induced rectification.

Changes made to the manuscript:

Page 7, Line 130-140: Notably, the Arrhenius plot in Fig. S14b exhibits a nonlinear behavior: at high temperatures, the current decreases exponentially with temperature, while at low temperatures it saturates to a temperature-independent plateau, consistent with a transition from thermally activated hopping to coherent off-resonant tunneling as molecular vibrations freeze out. This behavior does not contradict the involvement of molecular orbitals in transport but rather reflects the vibrational broadening of the molecular level at higher temperatures. Regarding the *I-V* asymmetry in Fig. 2a, the relatively weak rectification observed within the measured bias range (±0.5 V) arises because the molecular level remains within the bias window for both polarities; however, the strong ON-OFF transistor switching is governed by gate-controlled alignment of the molecular level relative to the electrode Fermi levels, which is independent of the degree of bias asymmetry.

- A more detailed explanation on how the gate voltage is applied via the IL medium is needed. Is there an external reference electrode immersed in the IL drop? This is not clear from the device schemes.

Response: We thank the reviewer for pointing out this lack of clarity. For our wafer-scale devices, the gate voltage was applied by directly immersing a tungsten probe tip into the ionic liquid (IL) droplet. Electrical measurements were performed using a Keysight B2912 Source/Measure Unit. The common ground was connected to the bottom electrode (Au), while two high-voltage sources were connected to the top electrode (graphene) and the tungsten gate probe, respectively. No external reference electrode was used. For smaller, individual devices,

we also employed evaporated gold electrodes in contact with the IL for gating.

Changes made to the manuscript:

Page 5, Line 86-90: Upon applying a gate voltage V_{gs} via a tungsten probe (or a metal electrode) in direct contact with the ionic liquid, with no external reference electrode, the redistribution of charge in the ionic liquid generates strong electric field (only partially screened by SLG) in the SAMs, providing the transistor conductance switching by orbital gating.

- Transistor curves in Figs. 3a and c show a general lift as the gate voltage increases. While this is clear of the ON state which is based on a hopping mechanism, the increasing "leakage" current observed in the tunnelling-based OFF state is not so obvious. Explain please.

Response: We thank the reviewer for this question, which touches upon a key aspect of the transport mechanism. As illustrated schematically in Figure 3i, in the tunneling-based OFF state, the molecular orbital is gated out of the resonance window with the source and drain electrode Fermi levels. However, due to the finite coupling between the molecule and the electrodes, the gate voltage modulation has a physical limit; the energy offset cannot be increased indefinitely. Consequently, charge transport in this regime is dominated by off-resonant tunneling, which results in a small, non-zero saturation current. This is in contrast to a symmetric two-terminal junction (like alkanethiols), where the bias voltage itself directly distorts the tunneling barrier, leading to a continuous increase in tunneling current with bias. In our three-terminal device, once the OFF state is achieved, the small residual "leakage" current is primarily determined by this off-resonant tunneling process and shows a much weaker dependence on the gate voltage, which is consistent with our observations.

- The poor ON-OFF behaviour recorded for the C8 control is not so obvious to me as in Fig. S20 a significant ON-OFF ratio is recorded. This clashes with the idea of a molecular component providing essentially electron tunnelling through out all voltage window. Please explain.

Response: We agree with the reviewer that the ON-OFF ratio for the C18 control sample is observable, but it is still far below our LUMO- and HOMO-transistors. We interpret this finite ratio as arising from two combined effects. First, as observed in previous studies, alkanethiols can induce a weak p-type doping effect on the single-layer graphene (SLG) electrode, which

can slightly modulate the overall device current. Second, and more importantly, even though the HOMO and LUMO levels of alkanethiols (C18) are far from the Fermi level of the electrodes, the electric field from the gate, which penetrates through the graphene, can still modulate the molecular energy landscape. As demonstrated in the framework for tunneling transistors by Duan et al. (Sci. Adv., 2018, 4, eaat8237), a positive gate voltage can lower the LUMO, and a negative gate voltage can raise the HOMO. In both cases, this field effect brings one of the molecular orbitals slightly closer to the Fermi level compared to the zero-gate-voltage condition, leading to a small increase in the transmission function and thus a measurable, albeit modest, ON-OFF ratio. For C18, this ratio is ~10. We have revised the discussion of Figure S20 to incorporate this explanation more clearly.

Changes made to the supporting information:

Page 35, Line 393-405: We have incorporated this discussion into the relevant section of the SI.

- While the conducted study here points to an all-electric operation principle for the molecular transistor, given the structural complexity of the molecular layers, likely defective, charging effects induced by the voltage gate could possibly lead to structural changes in the layer due to electrostatic effects which would point to structurally-induced gating effects in the transistor operation. The above discussion MUST be part of the conclusions.

Response: We thank the reviewer for this critical and insightful comment. We fully agree that charge-induced structural changes or conformational shifts within the SAM, which could lead to a structurally-induced gating effect, are a possibility that must be considered. To rule out such effects in our study, we performed several control experiments. First, we measured the transfer characteristics at different voltage sweep rates and observed no significant hysteresis, suggesting that the gating effect is primarily electronic and not due to slow ionic motion or molecular reconfiguration. Second, we employed molecules with similar energy levels but different structures to validate that the observed trends in transistor behavior are consistent with our energy-level-based design strategy. However, we acknowledge that these are indirect proofs. We have now added a short discussion to the result section, explicitly addressing the possibility of structurally-induced gating and explaining how our experimental evidence points towards an all-electric operation principle. We thank the reviewer for ensuring we address this important point.

Changes made to the manuscript:

Page 10, Line 184-192: Furthermore, to rule out the possibility of structurally-induced gating effects, we performed transfer characteristic measurements at varying voltage sweep rates and observed no significant hysteresis, indicating that the gate modulation is predominantly electronic and not due to slow ionic motion or molecular conformational changes within the SAM. To validate the universality of the molecular transistor design presented in this work, we tested two additional SAMs, including Fc-SH (ferrocene derivative) and PDI-SH (perylene diimides derivative) (Fig.S22). As shown in Sections S3, Fc-SH, with near-E_F HOMO at -4.97 eV, exhibits a HOMO-type transistor response similar to exTFF-SH, while PDI-SH, with near-E_F LUMO at -3.95 eV, shows the similar characteristics as C_{60}-SH.

Response to Reviewer Comments

Reviewer #3 (Remarks to the Author):

This revised manuscript "High-performance Microelectronic-integratable Molecular Transistors" by Y. Xie, et.al, reports ionic-liquid-gated molecular transistors based on Au–SAM/single-layer graphene (SLG) vertical heterostructures, demonstrating high ON/OFF ratios (>10^4), stable operation at and above room temperature, and wafer-scale device integration. The authors further implement logic gate functionality, highlighting the potential of this system for bridging molecular electronics with microelectronic compatible device platforms. The concerns raised by the reviewers are well addressed in the revised version.

While the manuscript is already of high quality and close to publication standard, a minor refinement in the presentation could further enhance its clarity and rigor. In particular, even though the expanded control experiments strongly support the interpretation that the gate modulation is dominated by molecular orbital alignment, the current evidence is better described as being consistent with this mechanism rather than strictly excluding all alternative contributions. A slight moderation of the language (for example, replacing "rule out" in line 184 with "consistent with" or "suggest") and a brief acknowledgment of possible secondary contributions from graphene-related effects would significantly improve the balance and precision of the discussion.

I therefore recommend acceptance after addressing these above-mentioned minor concerns.

Response: We thank the reviewer for the positive assessment and for the constructive suggestion. We agree that the language should be more balanced. In the revised manuscript, we have replaced turn down some claims, such as "rule out" changing to "consistent with" or "suggest", and we have removed some overly absolute adjectives. At the same time, we have added a brief acknowledgment that the single-layer graphene plays a critical role in the vertical heterostructure and that secondary contributions from graphene-related effects cannot be strictly excluded. These changes improve the precision and rigor of the discussion. Thank you again for your valuable feedback.

Changes made to the manuscript:

Page 7, Line 130: indicating→suggesting

Page 7, Line 130: arises because→can be attributed to

Page 9 Line 175: strongest increase→a pronounced increase

Page 10 Line 185: confirm→are consistent with

Page 10, Line 187: to rule out→to assess

Page 10, Line 189: indicating→suggesting; and not due to→,with no clear indication of

Page 11, Line 209: is the determining factor→appears to be the primary factor

Changes made to the manuscript:

Page 10, Line 198: In addition, the graphene top electrode may also contribute to the observed field-effect characteristics. Molecular adsorption can induce p- or n-type doping in graphene, while its Fermi level is simultaneously tunable by the gate electric field. The energy level alignment and electronic coupling at the graphene–molecule interface further influence charge injection and transport. Therefore, the device response likely reflects a combined effect of molecular electronic structure and graphene-assisted modulation.

Reviewer #4 (Remarks to the Author):

The authors have carefully addressed all the concerns raised in the previous review round. I have no further questions or comments. In my opinion, the manuscript is now suitable for publication in its present form, and I recommend acceptance.

Response: We thank the reviewer for the agreement of the publication.

Reviewer #5 (Remarks to the Author):

I have read the responses given to my queries and to those from other reviewers, and I am happy with the answers provided and the modifications introduced in the manuscript accordingly,

which have now significantly improved the clarity of many technical aspects related to the work.

Thanks

Response: We thank the reviewer for the agreement of the publication.